PHYSICAL SCIENCE

Superradiance on the millihertz linewidth strontium clock transition

Matthew A. Norcia,* Matthew N. Winchester, Julia R. K. Cline, James K. Thompson

Laser frequency noise contributes a significant limitation to today's best atomic clocks. A proposed solution to this problem is to create a superradiant laser using an optical clock transition as its gain medium. This laser would act as an active atomic clock and would be highly immune to the fluctuations in reference cavity length that limit today's best lasers. We demonstrate and characterize superradiant emission from the millihertz linewidth clock transition in an ensemble of laser-cooled ^{87}Sr atoms trapped within a high-finesse optical cavity. We measure a collective enhancement of the emission rate into the cavity mode by a factor of more than 10,000 compared to independently radiating atoms. We also demonstrate a method for seeding superradiant emission and observe interference between two independent transitions lasing simultaneously. We use this interference to characterize the relative spectral properties of the two lasing subensembles.

INTRODUCTION

Optical atomic clocks have recently achieved fractional instability in their ticking rate of a few parts in 10^{18} (*1*–*4*). Significant improvements in the accuracy, precision, and bandwidth of clocks and the lasers used to probe them would significantly advance a broad range of science and technology, including tests of general relativity (*5*), proposed gravitational wave detection (*6*), searches for variations of fundamental constants (*7*) and new gravitational couplings (*8*), searches for dark matter (*9*, *10*), gravitational potential sensing for geodesy (*5*), stabilization of future quantum networks (*11*), and explorations of quantum many-body physics (*12*, *13*).

At the heart of these optical clocks are atoms like ^{87}Sr, which has a quantum state with a long decay lifetime of roughly 150 s (*14*, *15*). The inverse lifetime of this state corresponds to a frequency linewidth of 1 mHz, which is more than 10^9 times narrower than typical optically excited states. This linewidth relative to the frequency of the optical photon emitted when the atom decays corresponds to a large fundamental quality factor $Q = 4 \times 10^{17}$, which is a key figure of merit for a clock. However, because of frequency instability in the lasers used to probe the atoms, today's best clocks can only resolve a much broader linewidth, and therefore a lower Q—the atoms are more precise than the lasers used to measure them (*3*).

For decades, heroic efforts have been made to reduce the frequency linewidth of conventional lasers by stabilizing their frequency to mechanically stable optical reference cavities (*16*, *17*). The primary limitation of this approach is the thermal Brownian motion of the cavity mirror spacing that produces noise in the cavity's resonance frequency (*18*, *19*). Cryogenic single-crystal optical cavities are being explored as a way to mitigate these effects (*20*).

Here, we present the first key step toward a radically different approach to narrow-linewidth lasers by directly collecting light emitted from a long-lived quantum state (*21*, *22*). In such a laser, the role of the optical cavity in determining the lasing frequency is highly suppressed. This would lead to a laser of the order 10^5 times less sensitive than a conventional laser to thermal and technical sources of cavity frequency noise (*23*, *24*).

In this approach, the long lifetime becomes a serious challenge. Typically, photons are emitted far too slowly to serve as a useful phase or frequency reference and are emitted into all directions, making them difficult to utilize. To overcome these limitations, we achieve pulsed superradiant lasing for the first time on an ultraweak optical clock transition: the millihertz linewidth $^3P_0$-to-$^1S_0$ clock transition at 698 nm in ^{87}Sr. Superradiant stimulation of photon emission allows us to efficiently collect photons emitted from the 150-s lifetime state in under 100 ms. The emitted laser light both serves as an absolute frequency reference and offers a new path toward lasers with linewidths at or below the millihertz level (*22*), orders of magnitude narrower than what has previously been achieved with traditional optical reference cavities (*17*).

To achieve lasing, the collectively enhanced emission rate from the atoms must be made larger than atomic decoherence rates, a stringent requirement for this ultraweak transition. To increase the collectively enhanced decay rate, we trap the atoms within a high-finesse optical cavity (Fig. 1A), effectively increasing the optical depth of the atomic ensemble. To suppress atomic decoherence, we rely on the techniques used to provide long coherence times in optical lattice clocks (*25*, *26*); by laser cooling and confining the atoms along the cavity axis with a magic-wavelength optical lattice, we eliminate first-order Doppler shifts in the direction of emission without imposing large shifts to the lasing transition frequency.

In conceptually related work, Raman transitions between ground hyperfine states of rubidium have enabled proof-of-principle explorations of lasing in the deep bad-cavity or superradiant regime (*23*, *27*), in which the bandwidth of the laser's gain medium (the atomic transition) is much narrower than that of the laser's optical cavity. However, because the frequency stability of a Raman laser is limited by the stability of the lasers used to induce optical decay between ground states, this system is not suitable for a frequency reference. For this, a true narrow-linewidth optical transition is required. In addition, the clock transition used here is orders of magnitude narrower than the effective decay linewidth used in Raman systems.

Superradiance has been studied in a variety of other more broadband systems, including thermal molecular and atomic gasses (*28*, *29*), Rydberg atoms (*30*), atoms trapped near photonic crystals (*31*), ions (*32*), artificial atoms (*33*), and other Raman systems (*34*–*36*). More generally, collective interactions mediated by the 7.5-kHz linewidth dipole-forbidden $^3P_1$-to-$^1S_0$ transition in ^{88}Sr have been studied in the context of lasing, cavity quantum electrodynamics (QED), and collective scattering (*24*, *37*–*40*). This work pushes into a new regime, exploring

JILA, NIST, and Department of Physics, University of Colorado, Boulder, CO 80302, USA.
*Corresponding author. Email: matthew.norcia@colorado.edu

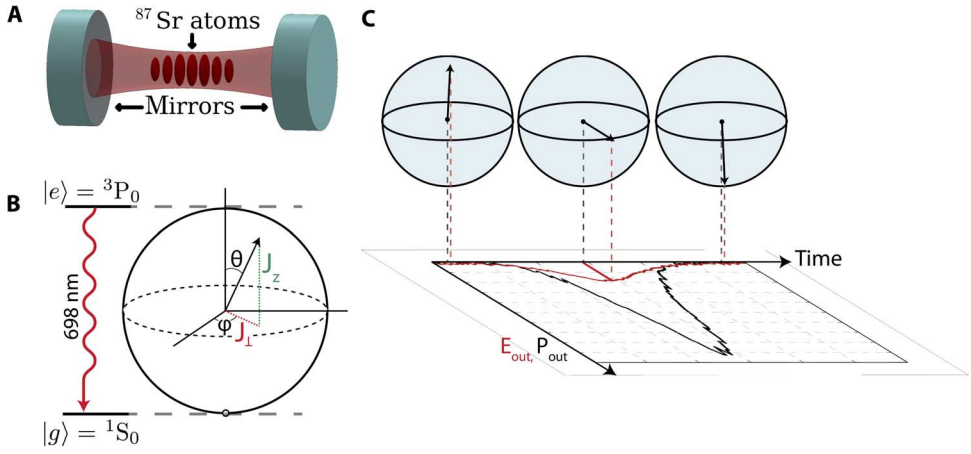

Fig. 1. Experimental overview. (**A**) Our system consists of an ensemble of up to $N = 2.5 \times 10^5$ laser-cooled ^{87}Sr atoms confined in a magic-wavelength optical lattice within a high-finesse ($F = 2.4 \times 10^4$; linewidth, $\kappa = 2\pi \times 160$ kHz) optical cavity. (**B**) The atoms undergo pulsed superradiant lasing on the $^3P_0$-to-$^1S_0$ optical clock transition that has a natural decay time of 150 s or an equivalent linewidth of 1 mHz. The state of the atomic ensemble can be represented by a collective Bloch vector (explained in the text). (**C**) Representation of a superradiant pulse on the Bloch sphere. The Bloch vector behaves like a highly damped pendulum that starts inverted at the north pole of the Bloch sphere (excited state). Quantum fluctuations disturb the system from its unstable equilibrium position, causing the Bloch vector to swing down the Bloch sphere, emitting peak radiation at the equator, and ultimately relaxing to the south pole (ground state), as inversion is lost. The radiated electric field (red trace) is proportional to the perpendicular projection of the Bloch vector, $J_\perp$, which at its peak is proportional to N. The radiated power (black trace) is proportional to the square of the radiated electric field, and at its peak is therefore proportional to N^2. This is one way to understand the origin of the collective enhancement in emission rate. The black output power trace on the projection plane is actual data.

collective interactions mediated by a transition nearly seven orders of magnitude weaker than even that weak transition.

Experimental system

Our experimental system consists of up to $N = 2.5 \times 10^5$ ^{87}Sr atoms cooled to 10 μK and tightly trapped along the axis of a high-finesse ($F = 2.4 \times 10^4$; linewidth, $\kappa = 2\pi \times 160$ kHz) optical cavity by an optical lattice. The lattice is near the magic wavelength of 813.4274 nm, for which the frequency shift of the two clock states is equal, making the transition frequency independent of lattice intensity (*25*). The interaction between the atoms and cavity mode can be characterized by the cooperativity parameter C of cavity QED. In our system, the peak single-particle cooperativity parameter is $C = 0.41$ (assuming a Clebsch-Gordan coefficient of 1). This number represents the relative probability that an atomic excitation leaves the system as a photon transmitted through a cavity mirror versus into free space. For a collective excitation of N atoms, this ratio is enhanced to ~NC. For our typical atom numbers, this means that an atom is far more likely to emit a photon into the cavity mode than into free space.

The state of the atomic ensemble can be represented by a collective Bloch vector, which is the vector sum of the Bloch vectors of the N individual atoms. This is illustrated in Fig. 1B. An atom in the excited state, $|e\rangle$ ($^3P_0$), has a Bloch vector pointing up, whereas an atom in the ground state, $|g\rangle$ ($^1S_0$), has a Bloch vector pointing down. An atom in an equal superposition of $|e\rangle$ and $|g\rangle$ corresponds to a Bloch vector on the equator of its Bloch sphere, with azimuthal phase φ determined by the phase of its superposition $|g\rangle + e^{i\varphi}|e\rangle$. To account for the spatial distribution of the atoms, we define the phase of each atom relative to the phase of a cavity mode resonant with the $|e\rangle$ to $|g\rangle$ transition, evaluated at the location of each atom. A collective Bloch vector on the equator of the Bloch sphere corresponds to each atom in a superposition of $|e\rangle$ and $|g\rangle$, with the appropriate phases to collectively radiate into the cavity mode.

The atoms radiate an electric field into the cavity at a rate proportional to $J_\perp$, the magnitude of the projection of the Bloch vector onto the equatorial plane of the Bloch sphere. The collective enhancement of emission results from the fact that the power radiated is proportional to the square of the electric field. Because the electric field is proportional to the atom number N, the radiated power scales as N^2 (*41*). The electric field radiated into the cavity acts on the atoms by causing rotation of the Bloch vector about an axis in the equatorial plane of the Bloch sphere by a rate proportional to $\sqrt{M_c}$, where M_c is the average number of photons in the cavity. This is the mechanism of stimulated emission in the superradiant regime. For an ensemble whose Bloch vector lies in the northern hemisphere of the Bloch sphere, this leads to positive feedback for emission. The atoms will radiate into the cavity, and the radiated electric field will then cause the Bloch vector to tip further from the north pole and thus to radiate more strongly. The result is a pulse of light that builds up gradually, reaches a peak in power as the Bloch vector passes the equator, and falls to zero as the atoms reach the ground state (Fig. 1C).

Observation of superradiant pulses

To observe superradiant pulses, we prepare atoms in $|e\rangle$, the nuclear $F = 9/2$, $m_f = 9/2$ sublevel of $^3P_0$. We first optically pump the atoms to $|g\rangle$, the $F = 9/2$, $m_f = 9/2$ sublevel of $^1S_0$, and then adiabatically transfer up to 75% of the atoms to $|e\rangle$ using a frequency-swept 698-nm transfer beam applied through the cavity. To prepare the atoms with full inversion (no atoms in $|g\rangle$) and ensure that the laser pulses are initiated by quantum noise rather than residual atomic coherence associated with the adiabatic transfer process, we then briefly apply lasers to the dipole-allowed $^1S_0$-to-$^1P_1$ transition to heat any atoms remaining in the ground state out of the lattice. The state preparation process is described in more detail in the Supplementary Materials. When all atoms are initially prepared in $|e\rangle$, we observe collectively enhanced decay on the clock transition.

Both quantitative and qualitative features of the collectively enhanced emission are markedly different from that of independent atoms. Not only does the collective enhancement lead to an emission rate into the cavity mode of up to 10^4 times greater than that of independently emitting atoms, but also the functional form of the decay versus time is distinctly

nonexponential. Figure 2A shows the photon output rate R for four representative pulses recorded with different initial atom numbers. Because the rate of collectively enhanced emission per atom scales with N, for higher atom numbers the pulses appear sooner, have shorter duration, and have a higher peak power than for lower atom numbers.

Figure 2B shows the characteristic N^2 scaling of the peak output power R_{peak} versus atom number that one expects for superradiance. In the presence of decoherence or atom loss, the atom number must exceed a threshold N_t for superradiance to occur. N_t is set by the requirement that the collectively enhanced decay rate exceeds the atomic decoherence rate. Above this threshold, we predict that $R_{peak} = \frac{1}{4\xi} N_x^2 C\gamma$, where $N_x = N - N_t$ is the total number of atoms in the lattice N in excess of the threshold atom number. The inhomogeneous coupling of the atoms to the cavity mode is accounted for by the numerical factor $\xi \approx 2.95$. (See the Supplementary Materials for details and note that all following expressions account for this inhomogeneity.) From a fit of this form, we extract a fitted threshold of $N_t = 3.3 \times 10^4$ atoms. From the fitted N_t and known C and γ, the measured peak photon emission rate R_{peak} is 0.7(4) times the above predicted rate.

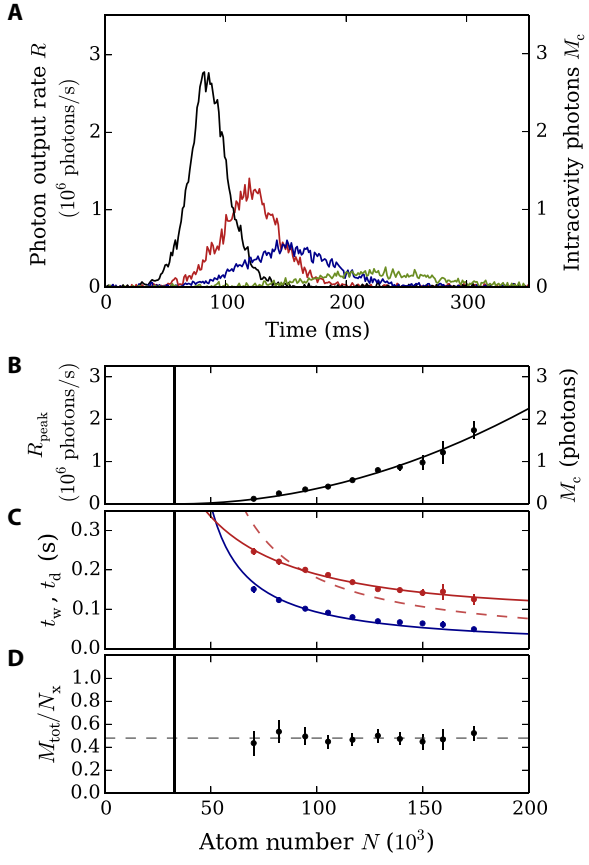

Fig. 2. Spontaneously generated superradiant pulses. (**A**) Representative single time traces of photon output rate R for pulses at different atom numbers $N \approx 100 \times 10^3$ (green), 125×10^3 (blue), 150×10^3 (red), and 200×10^3 (black). The equivalent average intracavity photon number is calculated on the right as $M_c = R/\kappa$. (**B**) Peak photon output rate, R_{peak}, versus initial total atom number. The black line is a quadratic fit to the output power. We observe a horizontal offset in the fit, indicating a threshold atom number N_t [black vertical line in (B) to (D)]. The threshold results from decoherence and atom loss and is a signature of lasing that would not be present for single-atom emission. (**C**) FWHM pulse duration t_w (blue) and delay of peak power t_d (red) versus initial total atom number. The blue line is a fit to the predicted functional form for the pulse duration, with N_t determined from the fit to R_{peak}. The dashed red line is a fit to the pulse delay, assuming that threshold is due to atomic homogeneous broadening without atom loss. The solid red line is a fit to the pulse delay, assuming that the threshold is set only by atom loss from the lattice. (**D**) The ratio of emitted photons M_{tot} to the number of atoms in excess of threshold N_x plotted versus atom number. The dashed line is the average ratio, showing that 48% of the atoms in excess of threshold participate in the superradiant pulse, largely independent of N.

The time duration of the superradiant pulse provides a measure of the collectively enhanced decay rate. The measured full width at half maximum (FWHM) versus atom number N is shown in Fig. 2C (blue points). We predict that the FWHM duration t_w of the pulse is given by $t_w \approx 7.05/(N_x C\gamma)$, such that the enhanced decay rate scales linearly with the excess atom number N_x. We fit this functional form (blue line) to the data, with the threshold held fixed to $N_t = 3.3 \times 10^4$ atoms from above. From this fit, we find that the measured FWHM is 1.4(7) times the predicted FWHM, given the known C and γ.

The measured delay time t_d of the peak in output power versus atom number N is shown in Fig. 2C (red points). In the presence of homogeneous broadening of the atomic transition, but with no atom loss, we expect the delay time to be given by $t_d \approx \frac{2(\ln N + \gamma_e)}{N_x C\gamma}$ (dashed red fit line with N_t fixed and C fitted), where $\gamma_e \approx 0.577$ is the Euler-Mascheroni constant. In the presence of atom loss from the lattice at rate γ_l, we observe a delay time in numerical simulations of the form $t_d \approx \alpha\gamma_l + \frac{2(\ln N + \gamma_e)}{NC\gamma}$, where α is a constant, a functional form which seems to better describe the data (solid red fit line with N_t fixed and C and α fitted.)

We define the number of atoms that participated in a superradiant pulse in terms of the integrated number of photons M_{tot} emitted from the cavity mode, that is, one photon equals one participating atom. Figure 2D shows the number of emitted photons per atom in excess of threshold, M_{tot}/N_x. We observe that above threshold, $M_{tot}/N_x = 0.48(15)$, independent of atom number. Because the peak photon output rate R_{peak} and pulse duration t_w scale as N_x^2 and $1/N_x$, respectively, we do not expect this quantity to depend on atom number. Inhomogeneous coupling to the cavity mode would predict $M_{tot}/N_x = 0.7$, partially accounting for the observed participation. Atomic collisions, which lead to an atom number–dependent contribution to N_t, may account for the additional reduction of participation. We may contrast this level of participation to the case where atoms emit independently: if there was no stimulation, only 0.1% of atoms would emit a photon into the cavity mode during our measurement time.

Seeding atomic coherence

Instead of preparing the atomic ensemble in the excited state with no initial coherence as before, we can terminate the adiabatic transfer process early and prepare the atoms in a superposition of $|g\rangle$ and $|e\rangle$. This seeds the collectively enhanced emission, and unlike in the nonseeded pulses of Fig. 2, we detect an immediate output of light from the cavity. Figure 3A shows a typical output trace resulting from terminating the adiabatic transfer with the Bloch vector just above the equator of the Bloch sphere.

Seeding the coherence in this manner also eliminates the threshold behavior observed in the spontaneously generated pulses of Fig. 2. Figure 3B shows the peak output power R_{peak} versus N for pulses seeded with the Bloch vector just above the equator of the Bloch sphere. These data are well described by a quadratic fit with no offset, that is, $N_t = 0$.

We view this technique for establishing collectively enhanced emission with no threshold or delay time to be a key tool for the development of superradiant sources. Here, being able to use these signatures of collectively enhanced emission to incrementally tune the system to meet

threshold was essential. More fundamentally, seeding allows collectively enhanced emission to be achieved in systems that are incapable of meeting threshold, but that may still be of metrological value. If superradiant pulses are used to stabilize the frequency of another laser, seeding could be used to reduce dead time that contributes to Dick noise aliasing (*42*).

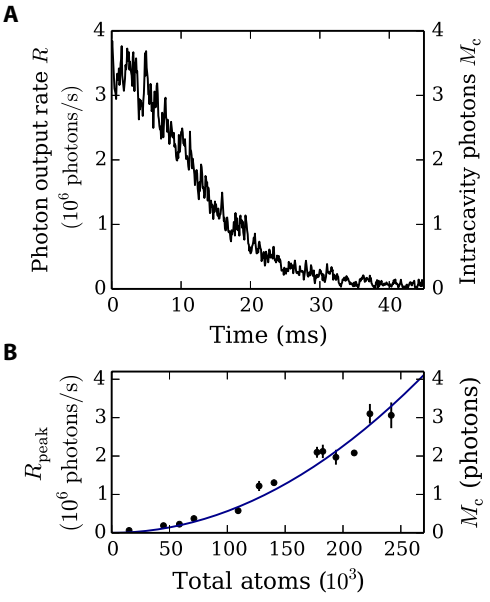

Fig. 3. Seeded superradiant pulses. (**A**) By terminating adiabatic transfer with atoms in a superposition of $|e\rangle$ and $|g\rangle$, we seed coherence in the atomic ensemble. Here, the atomic Bloch vector is rotated to just above the equator (that is, a small amount of initial inversion). Seeding leads to the immediate onset of superradiant emission, in contrast to the nonseeded pulses shown in Fig. 2 for which quantum noise seeds the coherence. (**B**) Peak output power for seeded pulses exhibits N^2 scaling. In contrast to the results in Fig. 2, seeded pulses exhibit a peak photon output rate consistent with no threshold ($N_t = 0$).

Simultaneous lasing on multiple transitions

For all preceding data, we applied optical pumping to primarily populate the $^1S_0$, $m_f = 9/2$ sublevel before adiabatic transfer, resulting in a single relevant lasing transition. We can deliberately reduce the efficiency of the optical pumping to populate both the $m_f = 9/2$ and $m_f = 7/2$ ground states and then adiabatically transfer the atoms into superpositions of ground and excited states with different m_f projections (represented in Fig. 4A). This creates two separate subensembles of atoms that interact with the same cavity mode but have slightly different transition frequencies (*43*, *44*). We observe a modulation in the output power at the magnetic field–induced frequency difference between the two transitions. This modulation is the result of interference between the fields radiated by the atoms lasing on the two transitions. Because more atoms are prepared in the m_f =9/2 sublevel, the total field radiated never goes through zero and the contrast of the modulation is not full.

Figure 4B shows the average of 20 time traces recorded under these conditions, illustrating that the phase of the modulation is the same between trials, a result of seeding coherence into the two transitions. To verify that the observed amplitude modulation is the result of beating between adjacent Zeeman transitions, we compute a Fourier transform of the emitted power (Fig. 4C) and fit the peak in the power spectrum that corresponds to the output power modulation. The frequency of this peak is plotted against our applied magnetic field in the inset of Fig. 4B. The slope and offset of beat frequency are consistent with the expected Zeeman splitting between the $m_f = 9/2$ and $m_f = 7/2$ transitions. The smaller peak near 400 Hz indicates that a smaller number of atoms have been left in the $m_f = 5/2$ state.

A Lorentzian fit to the peak in the average power spectrum returns a FWHM linewidth of 11 Hz, primarily reflecting the finite length of the pulse. Because many photons are detected in a trial of the experiment, we can fit the center of the Lorentzian peak with deviation much smaller than its width.

Treating this as a differential frequency measurement of two lasers, we compute a fractional Allan deviation of 2.6×10^{-15} at ≈ 2 s, the repetition rate of our experiment. Because many sources of frequency

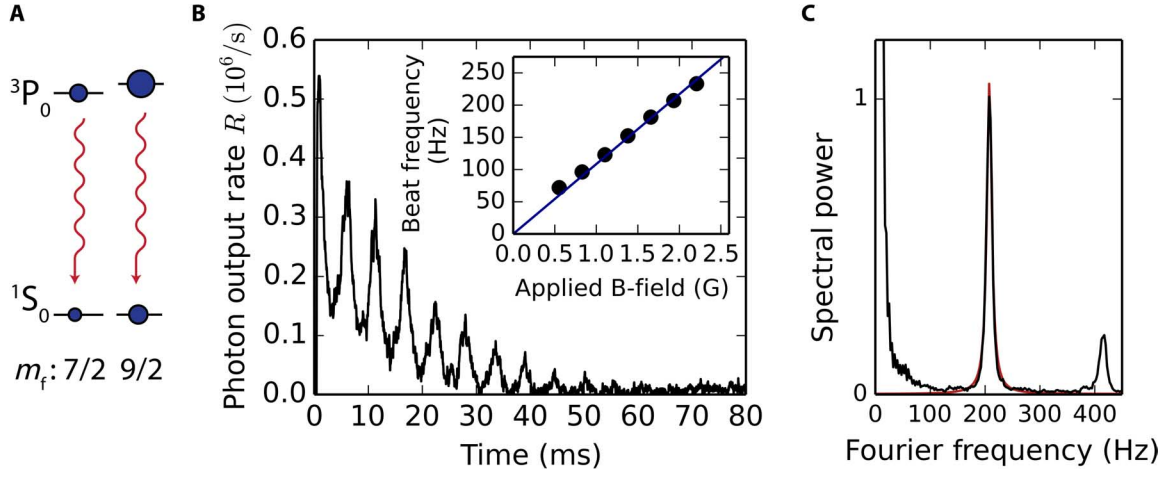

Fig. 4. Lasing on multiple transitions at the same time leads to beating in output power. (**A**) Atoms prepared in the $m_f = 9/2$ and $m_f = 7/2$ Zeeman sublevels radiate simultaneously into the cavity. (**B**) Interference between the electric fields radiated from the two transitions leads to a modulation of the output power. An average of 20 time traces is plotted, showing that the modulation has the same phase between trials of the experiment. (**C**) We compute a Fourier transform of an averaged time trace, showing a peak at the frequency splitting of adjacent Zeeman sublevels (≈200 Hz). The peak do to ≈400 Hz indicates that a smaller number of atoms have been prepared in $m_f = 5/2$. A Lorentzian fit to the average power spectrum (red line) returns a FWHM linewidth of 11 Hz due to the finite length of the pulse. The inset of (B) shows the center frequency of the Lorentzian fit versus applied magnetic field. The blue line shows the predicted splitting between adjacent Zeeman sublevels. G, gauss.

errors that are common-mode to the two lasing transitions are not captured by this measurement, this number does not indicate the ultimate performance of the system as a frequency reference. However, it does reflect a bound on its quantum-limited instability. To more fully characterize the spectral properties of the emitted light, including its sensitivity to effects that are common to the two transitions used here, it will be necessary to perform a comparison with an independent narrow-linewidth laser (*17*), which is a subject for future work.

Conclusion and outlook

We have demonstrated that an ultranarrow optical transition can be made to lase in a pulsed manner, with each atom emitting up to a single photon. In the future, it will be advantageous to operate in a continuous manner, with pump lasers applied to return the atoms to the excited state and a means of replenishing atoms lost to heating or collisions. An important property of a continuous superradiant laser is that the linewidth of the emitted light is not limited by the collectively enhanced decay rate, as would be the case for single-atom decay (*23*, *24*). Rather, the fundamental limit to the linewidth of the laser is of the order $C\gamma$, resulting from phase diffusion of the cavity field due to single-atom emission into the cavity mode.

A second key promise of a superradiant laser is its reduced sensitivity to fluctuations in the length of the laser cavity. The sensitivity of the lasing frequency to the cavity resonance frequency is quantified by a pulling coefficient $P = 2\gamma_\perp/(2\gamma_\perp + \kappa)$ (*23*, *24*, *45*). For a laser operating in the superradiant regime, $P \ll 1$. We assume that the dominant contribution to the broadening of the lasing transition, $\gamma_\perp$ is the pump process used to maintain inversion and that the rate of this pumping is tuned to be of the order $\frac{1}{8}NC\gamma$ (the maximum photon emission rate per atom in steady-state operation). For typical parameters used in this work, we would expect a pulling coefficient of the order 10^{-5}. This means that obtaining a laser stability at the millihertz level will require cavity stability at the 100-Hz level, which we believe will be achievable.

This work demonstrates that marked effects can result from collective interactions with an optical field, even when mediated by an optical transition so weak that it takes roughly 150 s to decay without stimulation. These interactions lead to stimulated emission in a regime where the cavity field is much shorter-lived than the coherence of the atomic ensemble, and open new avenues for the improvement of optical clocks, ultrastable lasers, and other atomic sensors along with their many applications.

MATERIALS AND METHODS

Subsequent laser cooling on the dipole-allowed $^1S_0$-to-$^1P_1$ transition at 461 nm and the dipole-forbidden $^1S_0$-to-$^3P_1$ transition at 689 nm allowed us to load a new ensemble of atoms into the optical lattice roughly every 2 s. The atoms were spread over roughly 1 mm along the cavity axis, corresponding to around 2000 occupied lattice sites.

At 698 (813) nm, the 4-cm-long cavity mode had a waist size of 74 (80) μm. At a typical lattice depth of 100 μK, the frequency of axial (radial) motion in the trap was 170 kHz (270 Hz), giving a Lamb-Dicke parameter $\eta = 0.16$ in the axial direction (*46*). For the $|e\rangle$ to $|g\rangle$ transition studied here, $C = 0.33$, and the single-photon Rabi frequency was $2g = 2 \times 2\pi \times 3.7$ Hz for a maximally coupled atom.

Detection was performed by coupling the output of the cavity to a single-mode optical fiber and detecting it on a single-photon counting module whose output was low-pass–filtered to provide a signal proportional to the photon emission rate from the cavity (more information on atomic manipulation and state preparation can be found in the Supplementary Materials).

SUPPLEMENTARY MATERIALS

Supplementary material for this article is available at http://advances.sciencemag.org/cgi/content/full/2/10/e1601231/DC1

Supplementary Text

fig. S1. Energy level diagram of relevant transitions.

REFERENCES AND NOTES

1. I. Ushijima, M. Takamoto, M. Das, T. Ohkubo, H. Katori, Cryogenic optical lattice clocks. *Nat. Photonics* **9**, 185–189 (2015).
2. B. J. Bloom, T. L. Nicholson, J. R. Williams, S. L. Campbell, M. Bishof, X. Zhang, W. Zhang, S. L. Bromley, J. Ye, An optical lattice clock with accuracy and stability at the 10^{-18} level. *Nature* **506**, 71–75 (2014).
3. N. Hinkley, J. A. Sherman, N. B. Phillips, M. Schioppo, N. D. Lemke, K. Beloy, M. Pizzocaro, C. W. Oates, A. D. Ludlow, An atomic clock with 10^{-18} instability. *Science* **341**, 1215–1218 (2013).
4. C. W. Chou, D. B. Hume, J. C. J. Koelemeij, D. J. Wineland, T. Rosenband, Frequency comparison of two high-accuracy Al^+ optical clocks. *Phys. Rev. Lett.* **104**, 070802 (2010).
5. C. W. Chou, D. B. Hume, T. Rosenband, D. J. Wineland, Optical clocks and relativity. *Science* **329**, 1630–1633 (2010).
6. A. Loeb, D. Maoz, Using atomic clocks to detect gravitational waves. ArXiv e-prints: 1501.00996 (2015).
7. T. M. Fortier, N. Ashby, J. C. Bergquist, M. J. Delaney, S. A. Diddams, T. P. Heavner, L. Hollberg, W. M. Itano, S. R. Jefferts, K. Kim, F. Levi, L. Lorini, W. H. Oskay, T. E. Parker, J. Shirley, J. E. Stalnaker, Precision atomic spectroscopy for improved limits on variation of the fine structure constant and local position invariance. *Phys. Rev. Lett.* **98**, 070801 (2007).
8. S. Blatt, A. D. Ludlow, G. K. Campbell, J. W. Thomsen, T. Zelevinsky, M. M. Boyd, J. Ye, X. Baillard, M. Fouché, R. Le Targat, A. Brusch, P. Lemonde, M. Takamoto, F.-L. Hong, H. Katori, V. V. Flambaum, New limits on coupling of fundamental constants to gravity using ^{87}Sr optical lattice clocks. *Phys. Rev. Lett.* **100**, 140801 (2008).
9. A. Arvanitaki, J. Huang, K. Van Tilburg, Searching for dilaton dark matter with atomic clocks. *Phys. Rev. D* **91**, 015015 (2015).
10. A. Derevianko, M. Pospelov, Hunting for topological dark matter with atomic clocks. *Nat. Phys.* **10**, 933–936 (2014).
11. P. Kómár, P. Kómár, E. M. Kessler, M. Bishof, L. Jiang, A. S. Sørensen, J. Ye, M. D. Lukin, A quantum network of clocks. *Nat. Phys.* **10**, 582–587 (2014).
12. G. Cappellini, M. Mancini, G. Pagano, P. Lombardi, L. Livi, M. Siciliani de Cumis, P. Cancio, M. Pizzocaro, D. Calonico, F. Levi, C. Sias, J. Catani, M. Inguscio, L. Fallani, Direct observation of coherent interorbital spin-exchange dynamics. *Phys. Rev. Lett.* **113**, 120402 (2014).
13. X. Zhang, M. Bishof, S. L. Bromley, C. V. Kraus, M. S. Safronova, P. Zoller, A. M. Rey, J. Ye, Spectroscopic observation of SU(*N*)-symmetric interactions in Sr orbital magnetism. *Science* **345**, 1467–1473 (2014).
14. S. G. Porsev, A. Derevianko, Hyperfine quenching of the metastable $^3P_{0,2}$ states in divalent atoms. *Phys. Rev. A* **69**, 042506 (2004).
15. R. Santra, K. V. Christ, C. H. Greene, Properties of metastable alkaline-earth-metal atoms calculated using an accurate effective core potential. *Phys. Rev. A* **69**, 042510 (2004).
16. B. C. Young, F. C. Cruz, W. M. Itano, J. C. Bergquist, Visible lasers with subhertz linewidths. *Phys. Rev. Lett.* **82**, 3799 (1999).
17. T. Kessler, C. Hagemann, C. Grebing, T. Legero, U. Sterr, F. Riehle, M. J. Martin, L. Chen, J. Ye, A sub-40-mHz-linewidth laser based on a silicon single-crystal optical cavity. *Nat. Photonics* **6**, 687–692 (2012).
18. K. Numata, A. Kemery, J. Camp, Thermal-noise limit in the frequency stabilization of lasers with rigid cavities. *Phys. Rev. Lett.* **93**, 250602 (2004).
19. M. Notcutt, L.-S. Ma, A. D. Ludlow, S. M. Foreman, J. Ye, J. L. Hall, Contribution of thermal noise to frequency stability of rigid optical cavity via hertz-linewidth lasers. *Phys. Rev. A* **73**, 031804(R) (2006).
20. C. Hagemann, Ultrastable laser with average fractional frequency drift rate below 5×10^{-19}/s. *Opt. Lett.* **39**, 5102–5105 (2014).
21. J. Chen, Active optical clock. *Chinese Sci. Bull.* **54**, 348–352 (2009).
22. D. Meiser, J. Ye, D. R. Carlson, M. J. Holland, Prospects for a millihertz-linewidth laser. *Phys. Rev. Lett.* **102**, 163601 (2009).
23. J. G. Bohnet, Z. Chen, J. M. Weiner, D. Meiser, M. J. Holland, J. K. Thompson, A steady-state superradiant laser with less than one intracavity photon. *Nature* **484**, 78–81 (2012).
24. M. A. Norcia, J. K. Thompson, Cold-strontium laser in the superradiant crossover regime. *Phys. Rev. X* **6**, 011025 (2016).

25. H. Katori, M. Takamoto, V. G. Pal'chikov, V. D. Ovsiannikov, Ultrastable optical clock with neutral atoms in an engineered light shift trap. *Phys. Rev. Lett.* **91**, 173005 (2003).
26. J. Ye, H. J. Kimble, H. Katori, Quantum state engineering and precision metrology using state-insensitive light traps. *Science* **320**, 1734–1738 (2008).
27. J. G. Bohnet, Z. Chen, J. M. Weiner, K. C. Cox, J. K. Thompson, Active and passive sensing of collective atomic coherence in a superradiant laser. *Phys. Rev. A* **88**, 013826 (2013).
28. N. Skribanowitz, I. P. Herman, J. C. MacGillivray, M. S. Feld, Observation of dicke superradiance in optically pumped HF gas. *Phys. Rev. Lett.* **30**, 309 (1973).
29. M. Gross, C. Fabre, P. Pillet, S. Haroche, Observation of near-infrared dicke superradiance on cascading transitions in atomic sodium. *Phys. Rev. Lett.* **36**, 1035 (1976).
30. M. Gross, P. Goy, C. Fabre, S. Haroche, J. M. Raimond, Maser oscillation and microwave superradiance in small systems of Rydberg atoms. *Phys. Rev. Lett.* **43**, 343 (1979).
31. A. Goban, C.-L. Hung, J. D. Hood, S.-P. Yu, J. A. Muniz, O. Painter, H. J. Kimble, Superradiance for atoms trapped along a photonic crystal waveguide. *Phys. Rev. Lett.* **115**, 063601 (2015).
32. B. Casabone, K. Friebe, B. Brandstätter, K. Schüppert, R. Blatt, T. E. Northup, Enhanced quantum interface with collective ion-cavity coupling. *Phys. Rev. Lett.* **114**, 023602 (2015).
33. M. Scheibner, T. Schimdt, L. Worschech, A. Forchel, G. Bacher, T. Paasow, D. Hommel, Superradiance of quantum dots. *Nat. Phys.* **3**, 106–110 (2007).
34. J. K. Thompson, J. Simon, H. Loh, V. Vuletić, A high-brightness source of narrowband, identical-photon pairs. *Science* **313**, 74–77 (2006).
35. C. W. Chou, S. V. Polyakov, A. Kuzmich, H. J. Kimble, Single-photon generation from stored excitation in an atomic ensemble. *Phys. Rev. Lett.* **92**, 213601 (2004).
36. T. Chaneliere, D. N. Matsukevich, S. D. Jenkins, S.-Y. Lan, T. A. B. Kennedy, A. Kuzmich, Storage and retrieval of single photons transmitted between remote quantum memories. *Nature* **438**, 833–836 (2005).
37. M. A. Norcia, J. K. Thompson, Strong coupling on a forbidden transition in strontium and nondestructive atom counting. *Phys. Rev. A* **93**, 023804 (2016).
38. P. G. Westergaard, B. T. R. Christenen, D. Tieri, R. Matin, J. Cooper, M. Holland, J. Ye, J. W. Thomsen, Observation of motion-dependent nonlinear dispersion-linewidth atoms in an optical cavity. *Phys. Rev. Lett.* **114**, 093002 (2015).
39. C. C. Kwong, T. Yang, M. S. Pramod, K. Pandey, D. Delande, R. Pierrat, D. Wilkowski, Cooperative emission of a coherent superflash of light. *Phys. Rev. Lett.* **113**, 223601 (2014).
40. S. L. Bromley, B. Zhu, M. Bishof, X. Zhang, T. Bothwell, J. Schachenmayer, T. L. Nicholson, R. Kaiser, S. F. Yelin, M. D. Lukin, A. M. Rey, J. Ye, Collective atomic scattering and motional effects in a dense coherent medium. *Nat Commun.* **7**, 11039 (2016).
41. M. Gross, S. Haroche, Superradiance: An essay on the theory of collective spontaneous emission. *Phys. Rep.* **93**, 301–396 (1982).
42. G. J. Dick, Local Ocillator Induced Instabilities in Trapped Ion Frequency Standards, *Proceedings of the 19th Annual Precise Time and Time Interval*, California, 1 to 3 December 1987.
43. J. M. Weiner, K. C. Cox, J. G. Bohnet, J. K. Thompson, Phase synchronization between two superradiant lasers. ArXiv e-prints, arXiv:1503.06464 (2015).
44. M. Xu, D. A. Tieri, E. C. Fine, J. K. Thompson, M. J. Holland, Synchronization of two ensembles of atoms. *Phys. Rev. Lett.* **113**, 154101 (2014).
45. S. J. M. Kuppens, M. P. van Exter, J. P. Woerdman, Quantum-limited linewidth of a bad-cavity laser. *Phys. Rev. Lett.* **72**, 3815 (1994).
46. G. Janik, W. Nagourney, H. Dehmelt, Doppler-free optical spectroscopy on the Ba^+ mono-ion oscillator. *J. Opt. Soc. Am. B* **2**, 1251–1257 (1985).

Acknowledgments: We gratefully acknowledge useful conversations with M. Holland, J. Ye, A. M. Rey, and T. Perkins, as well as technical assistance from J. Robinson and K. Mayer. Any mention of specific products in this work is given for technical information only and does not represent an endorsement by the National Institute of Standards and Technology (NIST). **Funding:** All authors acknowledge financial support from Defense Advanced Research Projects Agency Quantum-Assisted Sensing and Readout, Army Research Office, NSF Physics Frontiers Centers, and NIST. This work was supported by the NSF under grant no. 1125844. **Author contributions:** Design and construction of experimental apparatus and development of methods: M.A.N., M.N.W., and J.K.T. Data acquisition and analysis: M.A.N. Preparation and revision of manuscript: M.A.N., J.R.K.C., and J.K.T. Supervision of research and conception of experiment: J.K.T. **Competing interests:** The authors declare that they have no competing interests. **Data and materials availability:** All data needed to evaluate the conclusions in the paper are present in the paper and/or the Supplementary Materials. Additional data related to this paper may be requested from the authors.

Submitted 14 July 2016
Accepted 8 August 2016
Published 14 October 2016
10.1126/sciadv.1601231

Citation: M. A. Norcia, M. N. Winchester, J. R. K. Cline, J. K. Thompson, Superradiance on the millihertz linewidth strontium clock transition. *Sci. Adv.* **2**, e1601231 (2016).

Superradiance on the millihertz linewidth strontium clock transition

Matthew A. Norcia, Matthew N. Winchester, Julia R. K. Cline and James K. Thompson

Sci Adv **2** (10), e1601231.
DOI: 10.1126/sciadv.1601231